

# A Universal Electrode Approach for Automated Electrochemical Molecular Analyses

Mandy Lai Yi Sin, Vincent Gau, Joseph C. Liao, and Pak Kin Wong

**Abstract**—Transforming microfluidics-based biosensing systems from laboratory research into clinical reality remains an elusive goal despite decades of intensive research. A fundamental obstacle for the development of fully automated microfluidic diagnostic systems is the lack of an effective strategy for combining pumping, sample preparation, and detection modules into an integrated biosensing platform. Herein, we report a universal electrode approach, which incorporates dc electrolytic pumping, ac electrokinetic sample preparation, and self-assembled monolayer based electrochemical sensing on a single microfluidic platform, to automate complicated molecular analysis procedures that will enable biosensing applications in nontraditional health care settings. Using the universal electrode approach, major microfluidic operations required in molecular analyses, such as pumping, mixing, washing, and sensing, can be performed in a single platform. We demonstrate the universal electrode platform for detecting bacterial 16S rRNA, a phylogenetic marker, toward rapid diagnostics of urinary tract infection. Since only electronic interfaces are required to operate the platform, the universal electrode approach represents an effective system integration strategy to realize the potential of microfluidics in molecular diagnostics at the point of care. [2012-0310]

**Index Terms**—16S rRNA, electrochemical detection, electrokinetics, system integration, urinary tract infection.

## I. INTRODUCTION

**T**HE REALIZATION of fully integrated microfluidic systems for molecular analyses remains an elusive goal despite the intensive effort in the past decades [1]–[4]. Existing lab-on-a-chip devices often require bulky supporting equipments, and have limited applicability in non-traditional

health care settings (e.g., physicians' offices, emergency departments, and pharmacies) [5]. Currently, only few automated microfluidic systems exist for point-of-care molecular diagnostics, and most of them can only perform relatively simple molecular analysis procedures. The implementation of fully automated lab-on-a-chip systems is fundamentally hindered by the difficulty of integrating multiple fluid manipulation and molecular sensing modularities, such as external pumps, pressure sources, mixers, and biosensors, robustly and cost effectively. Effective system integration strategies are required to realize the potential of microfluidics in molecular analyses and other biomedical applications.

Sample preparation steps, such as mixing, washing, and concentration, are required in the assay protocol for molecular analyses. Several system integration approaches, such as digital, multiphase, magnetic, optofluidic, centrifugal, and electrokinetic techniques, have been developed for performing sample preparation procedures in microfluidic systems [6]–[9]. For point-of-care diagnostics, electrokinetics is one of the most promising platforms due to the cost effectiveness, simplicity in microelectrode fabrication, and advancement in portable electronic interface [10], [11]. Recent efforts in electrokinetics have allowed various fundamental microfluidic operations, such as mixing, concentration, and separation, to be performed in high conductivity, physiological fluids [12]–[16]. Furthermore, electrokinetics can be implemented conveniently with other MEMS components and represents a promising technology for microfluidic system integration.

An automated molecular analysis system also requires a sensing module. Among different transduction mechanisms, electrochemical biosensing is sensitive, specific, and rapid, and represents an attractive strategy for point-of-care diagnostics of infectious diseases, such as urinary tract infection (UTI), one of the most common bacterial infections [17], [18]. For instance, we demonstrated a self-assembled monolayer (SAM)-based electrochemical biosensor for detecting bacterial 16S rRNA and protein biomarkers [19]–[21]. We have also shown the implementation of *in situ* ac electrothermal flow (ACEF) induced mixing and on-chip heating on the electrochemical sensor [16]. ACEF is an electrohydrodynamic effect, which is particularly effective in high conductivity physiological and biological buffers, such as urine, plasma, and phosphate buffer [22], [23]. With the *in situ* enhancement strategy, the sensitivity of the assay can be enhanced over one order of magnitude and the diffusion limited incubation step can be accelerated with a six-fold reduction in the total assay

Manuscript received October 24, 2012; revised January 26, 2013; accepted March 6, 2013. Date of publication April 22, 2013; date of current version September 27, 2013. This work was supported in part by the National Institutes of Health under Grant 1U01AI082457-03 and Grant 2R44AI088756-03, in part by the National Institutes of Health Director's New Innovator Award under Grant 1DP2OD007161-01, and in part by the National Science Foundation under Grant 0930900. Subject Editor D. L. DeVoe.

M. L. Y. Sin was with the Department of Aerospace and Mechanical Engineering, University of Arizona, Tucson, AZ 85721 USA. She is now with the Department of Urology, Stanford University, Stanford, CA 94305 USA (e-mail: mandysin@stanford.edu).

V. Gau is with GeneFluidics, Inc., Irwindale, CA 91010 USA (e-mail: vgau@genefluidics.com).

J. C. Liao is with the Department of Urology, Stanford University, Stanford, CA 94305 USA (e-mail: jliao@stanford.edu).

P. K. Wong is with the Department of Aerospace and Mechanical Engineering, University of Arizona, Tucson, AZ 85721 USA (e-mail: pak@email.arizona.edu).

Color versions of one or more of the figures in this paper are available online at <http://ieeexplore.ieee.org>.

Digital Object Identifier 10.1109/JMEMS.2013.2253545

TABLE I  
SEQUENCES OF OLIGONUCLEOTIDE USED IN THIS WORK

Oligonucleotide	Sequence (5'-3')
EC471C	5'-CTGCGGGTAACTGCAATGAGCAAA-3'
EC447D	5'-GGTATTAACCTTACTCCCTTCCTC-3'

time [16]. Nevertheless, the electrochemical assay requires trained personnel to perform the assay steps. The requirement of multiple washing and mixing steps presents a significant challenge for the assay to be implemented in a fully automated fashion.

In this paper, we develop a universal electrode approach toward the implementation of fully integrated microfluidic biosensing systems. In particular, we incorporate electrolytic pumping, electrokinetic sample preparation, and amperometric sensing using a set of universal electrode array to implement the entire molecular assay automatically. We show that the electrolytic pump allows effective fluid delivery and washing, and ACEF enables mixing and assay enhancement directly on the electrochemical sensor electrode. Using pathogenic clinical isolates from patients, we demonstrate the applicability of the universal electrode approach for detecting bacterial 16S rRNA for infectious disease diagnostics.

## II. DESIGN AND FABRICATION

### A. Electrochemical Biosensor

The electrochemical biosensor consists of a concentric electrode design with working (W), auxiliary (A), and reference (R) electrodes (Fig. 1(a) and (b)). The sensor surface is modified with a SAM, which minimizes non-specific binding and reduces the background noise [24], [25]. The detection strategy involves sandwich hybridization of the target nucleic acid (16S rRNA) by a biotin-modified capture probe (EC471C) and a fluorescein-modified detector probe (EC447D) (Fig. 1(c)). The sequence was obtained from the NCBI database (Bethesda, MD), and the hybridization accessibility of the target sequence is evaluated using the Mfold server [26]. The sequences of oligonucleotide probes used are summarized in Table 1. The specificity of the probes has been verified in our previous studies [19]–[21]. The sensor surface is first immobilized with the biotinylated capture probes through streptavidin-biotin binding. Then, the bacterial 16S rRNA targets are allowed to hybridize with the capture probes and the detector probes in 1M phosphate buffer (Sigma-Aldrich, P3288) with 2.5% bovine serum albumin (Sigma-Aldrich, A7906). After hybridization, unbound targets and detector probes are washed away. The detection of the capture-probe-target-detector-probe hybrids is achieved through the binding of horseradish peroxidase (HRP)-conjugated anti-fluorescein antibodies (Roche, 11426338910) to the detector probes followed by another washing step for removing any unbound HRP.

Upon loading of the substrate  $H_2O_2$  with 3,3',5,5'-tetramethylbenzidine (TMB) (Neogen, 330176) as the electron transfer mediator, the HRP-catalyzed redox reaction is con-

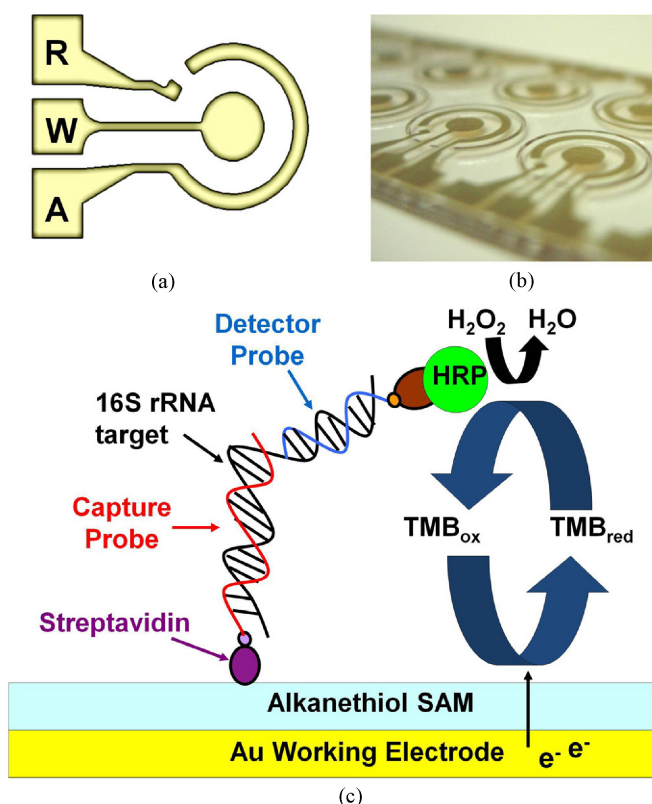
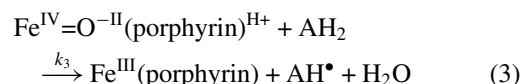
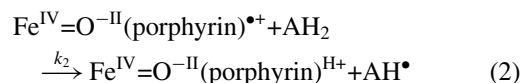
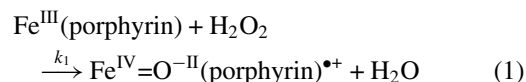


Fig. 1. Electrochemical biosensor for bacterial 16S rRNA. (a) Concentric electrode configuration for electrochemical sensing. (b) Photo of the concentric electrode. (c) Schematic of the sandwich binding scheme for detecting bacterial 16S rRNA toward urinary tract infection diagnostics.

verted to an amperometric signal. The reaction includes three irreversible steps:



The first step is a two electron oxidation/reduction reaction where  $H_2O_2$  is reduced to water and the enzyme is oxidized. The original form of HRP, which is the resting state ferric enzyme  $Fe^{III}$  (porphyrin), is oxidized by 1 equiv. of  $H_2O_2$ . An active intermediate, in which the iron is oxidized to a ferryl ( $Fe^{IV} = O^{-II}$ ) with one oxidizing radical ( $\bullet+$ ), is generated. The oxidized form of HRP is reduced back to its original form in the two following steps. The TMB molecule is used as the organic electron mediator ( $AH_2$ ) in our protocol, which is oxidized to a free radical ( $AH^{\bullet}$ ) in each step. To read the signal, the potential between the working and reference electrodes is fixed at -200 mV and the electroreduction current is recorded using a potentiostat (GeneFluidics, Inc.). The current is measured after 60 s when the HRP redox reaction reaches a steady state, which corresponds to number of HRP

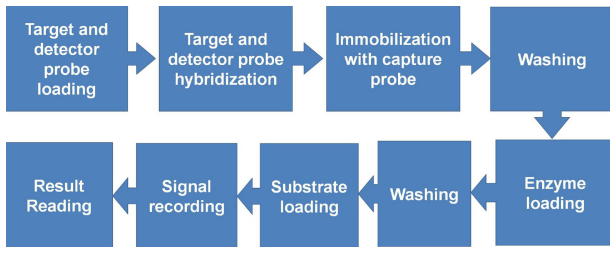


Fig. 2. Procedure of the electrochemical assay for detecting bacterial 16S rRNA.

molecules immobilized on the sensor surface. The protocol of the electrochemical assay for bacterial 16S rRNA in the integrated system involves: target and detector probe loading, target and detector probe hybridization, immobilization on the sensor surface, washing, enzyme loading, washing, substrate loading, signal recording and result reading (Fig. 2).

### B. AC Electrothermal Flow

Alternating current electrothermal flow (ACEF) is an electrohydrodynamic effect. It is operated with an ac voltage of frequency above 100 kHz where electrode polarization and ac electro-osmosis are negligible. When an electric field is applied in the fluid, temperature gradients can be induced near the electrode depending on the magnitude of the electric field and electric conductivity of the fluid, which results in permittivity and conductivity gradients. The interaction between these gradients and the electric field leads to net electrical force and bulk fluid motion. As thermal equilibrium can be achieved on the order of milliseconds in a typical microfluidic system, the effect of ACEF-induced fluid motion on thermal diffusion can be neglected. The simplified energy balance equation can be expressed as

$$k\nabla^2 T + \sigma E^2 = 0 \quad (4)$$

where  $E$  is the applied electric field.  $k$ ,  $T$ , and  $\sigma$  are the thermal diffusivity, temperature, and conductivity of the medium, respectively. The temperature rise in the medium due to joule heating can be estimated by

$$\Delta T = \sigma V_{rms}^2 / 8k. \quad (5)$$

The time-averaged electrothermal force per unit volume has been determined to be

$$\langle f_E \rangle = -\frac{1}{2} \left[ \left( \frac{\nabla \sigma}{\sigma} - \frac{\nabla \epsilon}{\epsilon} \right) \cdot \vec{E} \frac{\epsilon \vec{E}}{1 + (\omega\tau)^2} + \frac{1}{2} |\vec{E}|^2 \nabla \epsilon \right] \quad (6)$$

where  $\omega$  is the angular frequency of the applied electric field,  $\epsilon$  is the permittivity of the medium, and  $\tau = \epsilon/\sigma$  is the charge relaxation time of the medium. The first and second terms on the right hand side of (6) represent the Coulomb and the dielectric forces, respectively. Therefore, the magnitude of ACEF can be controlled by the applied voltage and frequency.

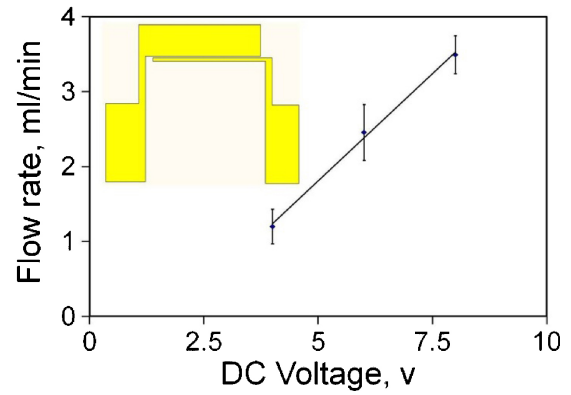
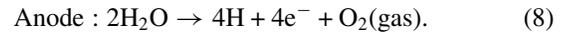
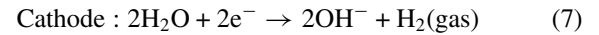


Fig. 3. Electrolytic micropump. Dependence of the pumping rate on the applied dc voltage. Data represent mean  $\pm$  SEM. Insert shows the design of the asymmetric electrode for pumping.

### C. Electrolytic Pumping

When a dc current is applied to the two metal electrodes, electrolysis occurs and the fluid is pushed by the electrolysis-bubble, which transforms electrochemical energy into mechanical energy. The decomposition potential for water electrolysis is  $-1.23$  V at  $25^\circ\text{C}$ . During electrolysis, hydrogen gas is produced at the cathode and oxygen gas is produced at the anode



Assuming that all the generated gases grow in the form of gas bubbles, the total volume of the gas generated through bubble nucleation can be evaluated according to the Faraday's law of electrolysis and the ideal gas law [27]. The electrolytic micropump consists of a pair of asymmetric electrodes with widths of  $100 \mu\text{m}$  and  $2000 \mu\text{m}$  (see inset of Fig. 3). The electrode is separated by a gap of  $100 \mu\text{m}$ . The electrodes were fabricated by evaporation of  $50 \text{ nm}$  of titanium (Ti),  $150 \text{ nm}$  of gold (Au), and  $50 \text{ nm}$  of titanium on glass substrate and were patterned by lift off. The sandwich Ti-Au-Ti structure is chosen to endure the high voltage for an extended period of time without deterioration of the electrodes in high conductivity media [14]. A function generator (HP, 33120A) was used to generate the dc voltage signal. The  $100 \mu\text{m}$  width electrode and the  $2000 \mu\text{m}$  width electrode were connected to the driving signal and the ground respectively. The dc voltage applied across the electrode was monitored by a digital storage oscilloscope (GW Instek, GDS-1102).

### D. Integrated Universal Electrode System

The universal electrode system consists of a set of seven micropump structures and an electrochemical sensing electrode located inside the mixing and sensing chamber (Fig. 4). A schematic of the fabrication process of the universal electrode system is shown in Fig. 5. The universal electrode array was fabricated by depositing  $50 \text{ nm}$  of titanium (Ti) and  $150 \text{ nm}$  of gold (Au). The sensing electrode was then covered with scotch tape before evaporating another  $50 \text{ nm}$  of

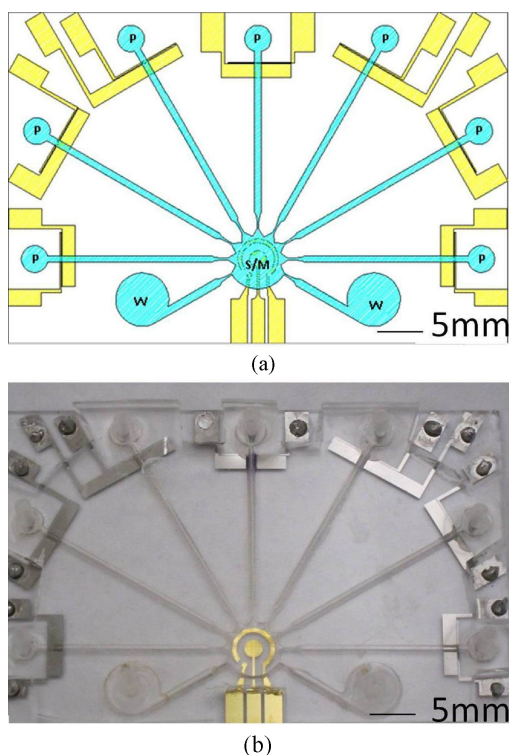


Fig. 4. Integrated universal electrode system. (a) Schematic of the integrated microfluidic system consisting of the asymmetric pumps (P), the waste chamber (W), and the concentric electrode for both mixing and sensing modules (S/M). (b) Photograph shows the schematic design of (a).

titanium (Ti) and was patterned by lift-off. For the fabrication of microchannel, the pattern was first engraved into an acrylic plate with a laser machining system (Universal Laser, Inc.). A rubber replica was then molded from the acrylic plate pattern using liquid urethane (Forsh Polymer Corp., 60A). The microchannel was then created by PDMS molding using the replica mold. The PDMS channel and the glass substrate with the universal electrode array was bound using atmospheric plasma treatment. The height of the microchannel is 800  $\mu\text{m}$ . The lengths of microchannels for pumping fluid to the central sensor chamber are between 25 and 29 mm and the width is 1 mm for all channels. As shown in Fig. 4, different solutions can be pumped from the asymmetric electrodes (P) toward the concentric electrode for both sample mixing (M) and sensing (S) modules for the electrochemical assay. The waste chamber (W) is used for waste solution storage after each washing step.

### III. RESULTS AND DISCUSSION

#### A. Electrolytic Pumping

The electrolytic pumping motion is driven by the asymmetric electrode pair. In our experiment, the conductivity of the electrolyte solution was adjusted to 1 S/m (similar to most biological buffers and physiological solutions) by the addition of sodium chloride (NaCl), which was used to evaluate the performance of the electrolytic micropump. The flow rate was studied and quantified as a function of the applied dc voltage (Fig. 3). A flow rate on the order of milliliter per

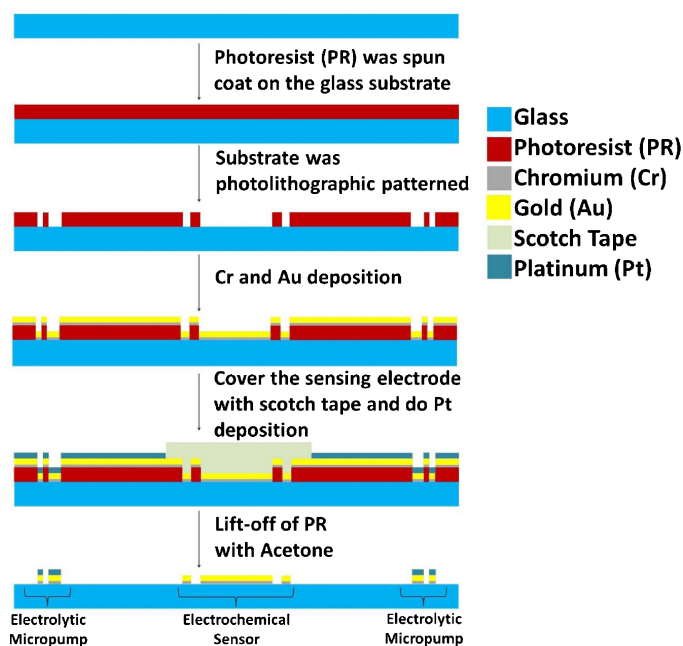


Fig. 5. Schematic of fabrication process of the universal electrode system on the glass substrate.

minute can be generated with only a few volts. Theoretically, the bubble growth rate should be linearly proportional to the applied current. As expected, the flow rate is found to be linearly proportional to the applied dc voltage. Extrapolation of the data reveals that the calibration curve intersects with the  $x$ -axis at  $\sim 1.8$  V. The value is in reasonable agreement with the decomposition potential for water electrolysis. With the optimized channel design and electrokinetic operating conditions, the flow rate obtained in this paper is from  $\sim 1$ –3.5 ml/min, which is at least one order of magnitude higher than typical bubble-actuated micropump [29], [30].

#### B. Microfluidic Operations With the Universal Electrode

To optimize the performance of the universal electrode array toward molecular analysis, color food dyes were applied for visualizing the pumping, mixing, and washing efficiencies inside the integrated microfluidic systems. Color food dyes and NaCl washing solutions with conductivity 1 S/m were loaded in the microchannels. Fig. 6(a) and (b) illustrates the motion of the food dyes toward the mixing and sensing chamber at the center of the integrated system when the electrolytic micropumps were actuated with 8V. The chamber was completely filled with the color dyes. An ac square waveform at 5  $V_{pp}$  and 200 kHz was then applied to the concentric electrode for mixing enhancement (Fig. 6(c) and (d)). The solutions were fully mixed in less than 3 min. The mixed dye solution in the chamber was then washed by the NaCl washing solution with the corresponding electrolytic micropump with dc 8 V. The dye solution was then pushed to the waste reservoirs. The solution in the sensing and mixing chamber could be completely removed in less than 4 min. It should be noted that the universal electrode platform does not require valves to control the fluid direction. During the washing step, the

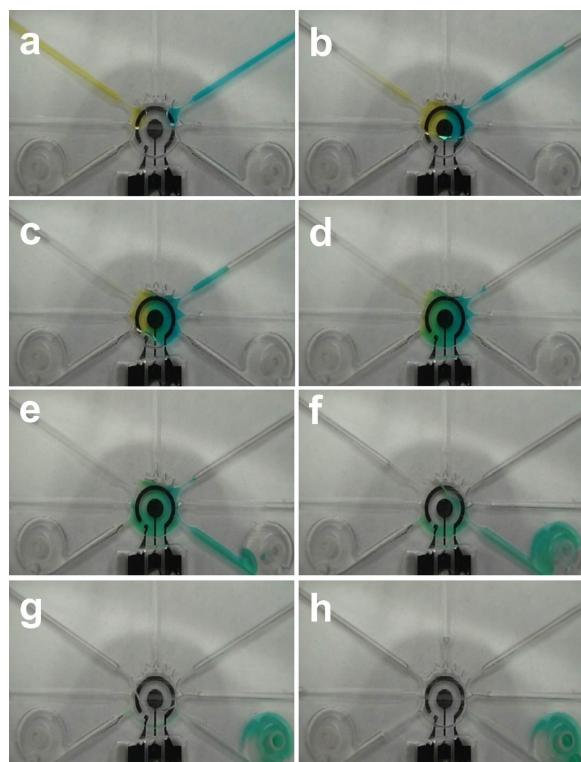


Fig. 6. Microfluidic operations in the universal electrode platform. (a)-(b) Electrolytic pumping of two color food dyes into the mixing and sensing chamber. (c)-(d) Electrokinetic mixing of the color food dyes is performed directly on top of the electrochemical sensing electrode. (e)-(h) Washing buffer is loaded into the channel using the electrolytic pump and delivered to the waste reservoirs.

dye and NaCl solutions were preferentially driven to the waste chambers instead of other pumping channels due to the low hydrodynamic resistances of the waste chambers, which are connected to open air. The high hydrodynamic resistance in the pumping channel is a result of the closed fluid connection, such as by connecting the inlet of the micropump with a syringe or a stopper. This valveless design significantly simplifies the system complexity and completely eliminates the requirement of external pressure sources, which will facilitate the implementation of the universal electrode system for point-of-care diagnostics in the future.

### C. Electrochemical Assays With the Universal Electrode

The integrated universal electrode system was applied to implement the electrochemical assay for detecting bacterial 16S rRNA. *E. coli* clinical isolates from UTI patients were chosen as the model system. All solutions were delivered using the electrolytic pump. The reagents include the bacterial lysate solution (*E. coli* mixed with the lysis buffer and 1 M NaOH), the detector probe solution, the enzyme solution, and the NaCl solution with conductivity 1 S/m (Fig. 7). The mixing and sensing chamber in the integrated system was washed only once with the NaCl washing solution after each incubation step. The hybridization between the 16S rRNA and the detector probe and the immobilization on the sensor surface by the capture probe were performed in the sensor chamber at the same time with and without ACEF enhancement. The results

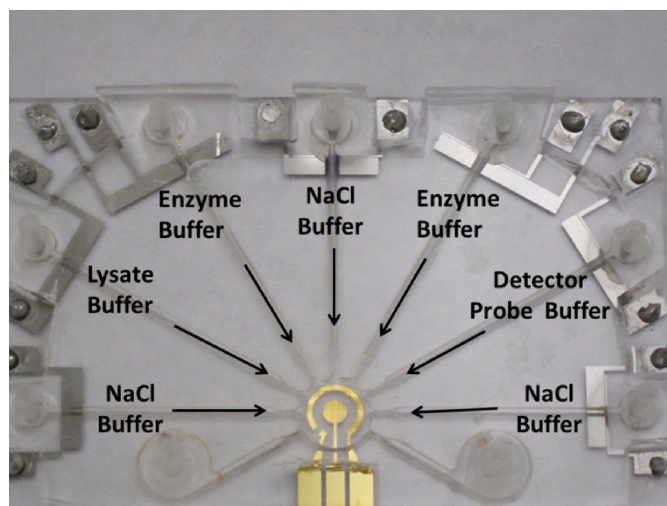


Fig. 7. Configuration of the universal electrode array for implementing the electrochemical assay for bacterial 16S rRNA.

were compared with the manual assay, which was performed manually with pipettes as in our previous studies [15]. In the manual assay, the sensing chamber was an opened acrylic well and was washed three times after each incubation step. The sample used in both the manual assay and the integrated system was the 16S rRNA target with concentration of  $4 \times 10^5$  cfu/sensor, which is a clinically relevant concentration for UTI diagnostics.

The performance of ACEF-induced mixing and heating for enhancing the 16S rRNA hybridization assay was first evaluated with the manual assay. The signals of the 16S rRNA assays performed with electrokinetic enhancement and by diffusion are shown in Fig. 8. The signal level with electrokinetic enhancement was increased by  $\sim 18$ -fold when compared to the value with diffusion (i.e., no electrokinetic enhancement), which was similar to the negative control due to the lack of an effective mixing mechanism. Moreover, electrokinetic enhancement significantly reduced the background noise in the negative control and improved the overall signal to noise ratio by  $\sim 30$ -fold. The noise reduction was a result of the elevated temperature and electrothermal stringency wash [16]. These results indicate that *in situ* electrokinetic enhancement can improve the signal-to-noise of the electrochemical assay.

In order to facilitate molecular analysis at the point of care, we have also demonstrated the ability to perform the electrochemical assay in the integrated system. The signals obtained from the integrated system were compared with the manual assay (Fig. 8). Examining the amperometric signals, we observed similar electrochemical behaviors in open wells and in encapsulated chambers, suggesting the same mechanism is governing the electrochemical performances as in our previous studies [24], [25]. With diffusion, the signal and noise levels were both increased in the integrated system when compared to the manual assay. The higher signal level can be understood by the shorter diffusion distance in the integrated system and the higher noise level could be due to the smaller number of wash and the lower washing efficiency in the integrated system. In contrast, with electrokinetics, the signal and noise level were both reduced in the integrated

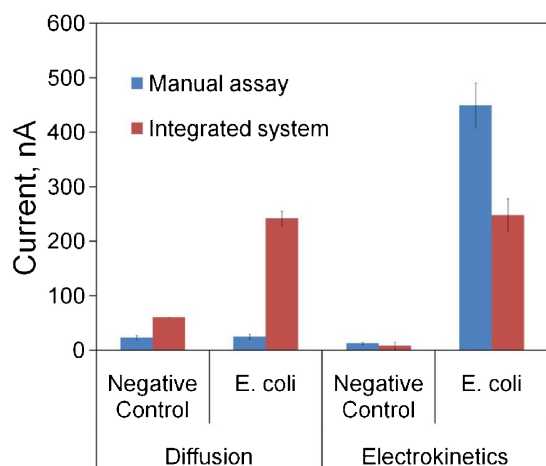


Fig. 8. Comparison of the electrochemical assays performed manually or by the integrated universal electrode system.

microfluidic system. It should be noted that the height of the integrated chip is 800  $\mu\text{m}$ , which is 2.5 times lower than that of the acrylic well in the manual assay (2 mm). The lower current level is likely due to the differences in channel geometries, which could affect the quasi-steady state substrate concentration. The smaller dimension may also play a role in the mixing effect, which is driven by the bulk fluid motion. Furthermore, the higher surface-to-volume ratio in the integrated system implies a larger temperature loss, which may modify the optimal condition for generating the electrothermal fluid motion for mixing and assay enhancement. Nevertheless, the signal-to-noise level is comparable between the integrated system and the manual assay in the experiment, which is  $\sim 30$ . These results demonstrate the applicability of the universal electrode approach in developing point of care device for electrochemical molecular diagnostics.

#### D. Discussion

In this paper, we demonstrate a universal electrode approach for microfluidics-based molecular biosensing. Using the universal electrode platform, all fundamental microfluidic operations, such as pumping, mixing, washing, enhancement and sensing, are integrated for molecular diagnostics. The asymmetric micropump design is capable of generating large volumetric flow rate, which is an order of magnitude higher than conventional electrolytic micropumps. Furthermore, the valveless design dramatically simplifies the system complexity and the cost of the system, which are essential for point-of-care diagnostics. The ability to directly perform *in situ* mixing and enhancement on the sensor electrode further simplify the system complexity, which is one of the major hurdles in realizing point-of-care diagnostics using MEMS based biosensing systems.

We have chosen UTI, which is the most common bacterial infection, diagnostics as the model system for demonstrating the universal electrode approach in point-of-care diagnostics. For clinical management of UTI, the existence and identification of the bacteria are some of the most critical aspects required to determine the proper treatment of the patients.

Since only electronic interfaces are required to implement the universal electrode approach, the universal electrode approach avoids bulky supporting equipment required in typical bio-analytical settings and will facilitates the implementation of microfluidics-based biochemical analysis in resource limited settings.

#### IV. CONCLUSION

In conclusion, we demonstrated a universal electrode approach for automating bioanalytical assays toward point-of-care diagnostics. Our work presents a novel approach for implementing both sample preparation and electrochemical sensing steps on the same universal electrode platform. With its general applicability and effectiveness, the universal electrode approach is anticipated to implement various microfluidics based bioanalytical assays for point-of-care diagnostics.

#### REFERENCES

- [1] M. L. Sin, J. Gao, J. C. Liao, and P. K. Wong, "System integration: A major step toward lab on a chip," *J. Biol. Eng.*, vol. 5, p. 6, May 2011.
- [2] G. Whitesides, "Solving problems," *Lab Chip*, vol. 10, no. 18, pp. 2317–2318, 2010.
- [3] M. L. Chiu, W. Lawi, S. T. Snyder, P. K. Wong, J. C. Liao, and V. Gau, "Matrix effect: A challenge toward automation of molecular analysis," *J. Assoc. Lab. Automat.*, vol. 15, no. 3, pp. 233–242, 2010.
- [4] T. H. Wang and P. K. Wong, "Transforming microfluidics into laboratory automation," *J. Assoc. Lab. Automat.*, vol. 15, no. 3, pp. A15–A16, 2010.
- [5] J. Kim, M. Junkin, D. H. Kim, S. Kwon, Y. S. Shin, P. K. Wong, and B. K. Gale, "Applications, techniques, and microfluidic interfacing for nanoscale biosensing," *Microfluid. Nanofluid.*, vol. 7, no. 2, pp. 149–167, 2009.
- [6] J. Gong and C. J. Kim, "Direct-referencing two-dimensional-array digital microfluidics using multilayer printed circuit board," *J. Microelectromech. Syst.*, vol. 17, no. 2, pp. 257–264, Apr. 2008.
- [7] S. Y. Teh, R. Lin, L. H. Hung, and A. P. Lee, "Droplet microfluidics," *Lab Chip*, vol. 8, no. 2, pp. 198–220, 2008.
- [8] T. Oka, K. Itani, Y. Taguchi, and Y. Nagasaka, "Development of interferometric excitation device for micro optical diffusion sensor using laser-induced dielectrophoresis," *J. Microelectromech. Syst.*, vol. 21, no. 2, pp. 324–330, Apr. 2012.
- [9] R. Gorkin, J. Park, J. Siegrist, M. Amasia, B. S. Lee, J. M. Park, J. Kim, H. Kim, M. Madou, and Y. K. Cho, "Centrifugal microfluidics for biomedical applications," *Lab Chip*, vol. 10, no. 14, pp. 1758–1773, 2010.
- [10] A. Ramos, H. Morgan, N. G. Green, and A. Castellanos, "AC electrokinetics: A review of forces in microelectrode structures," *J. Phys. D, Appl. Phys.*, vol. 31, no. 18, pp. 2338–2353, Sep. 1998.
- [11] P. K. Wong, T. H. Wang, J. H. Deval, and C. M. Ho, "Electrokinetics in micro devices for biotechnology applications," *IEEE/ASME Trans. Mechatronics*, vol. 9, no. 2, pp. 366–376, Jun. 2004.
- [12] S. Park, Y. Zhang, T. H. Wang, and S. Yang, "Continuous dielectrophoretic bacterial separation and concentration from physiological media of high conductivity," *Lab Chip*, vol. 11, no. 17, pp. 2893–2900, 2011.
- [13] A. Sonnenberg, J. Y. Marciniak, R. Krishnan, and M. J. Heller, "Dielectrophoretic isolation of DNA and nanoparticles from blood," *Electrophoresis*, vol. 33, no. 16, pp. 2482–2490, Aug. 2012.
- [14] J. Gao, M. L. Y. Sin, T. Liu, V. Gau, J. C. Liao, and P. K. Wong, "Hybrid electrokinetic manipulation in high-conductivity media," *Lab Chip*, vol. 11, no. 10, pp. 1770–1775, 2011.
- [15] J. Gao, R. Riahi, M. L. Sin, S. Zhang, and P. K. Wong, "Electrokinetic focusing and separation of mammalian cells in conductive biological fluids," *Analyst*, vol. 137, no. 22, pp. 5215–5221, Nov. 2012.
- [16] M. L. Y. Sin, T. T. Liu, J. D. Pyne, V. Gau, J. C. Liao, and P. K. Wong, "In situ electrokinetic enhancement for self-assembled-monolayer-based electrochemical biosensing," *Anal. Chem.*, vol. 84, no. 6, pp. 2702–2707, Mar. 2012.

- [17] J. Wang, "Electrochemical biosensors: Towards point-of-care cancer diagnostics," *Biosensors Bioelectron.*, vol. 21, no. 10, pp. 1887–1892, Apr. 2006.
- [18] K. E. Mach, P. K. Wong, and J. C. Liao, "Biosensor diagnosis of urinary tract infections: A path to better treatment?," *Trends Pharmacol. Sci.*, vol. 32, no. 6, pp. 330–336, Jun. 2011.
- [19] R. Mohan, K. E. Mach, M. Bercovici, Y. Pan, L. Dhulipala, P. K. Wong, and J. C. Liao, "Clinical validation of integrated nucleic acid and protein detection on an electrochemical biosensor array for urinary tract infection diagnosis," *Plos One*, vol. 6, no. 10, p. e26846, 2011.
- [20] K. E. Mach, R. Mohan, E. J. Baron, M. C. Shih, V. Gau, P. K. Wong, and J. C. Liao, "A biosensor platform for rapid antimicrobial susceptibility testing directly from clinical samples," *J. Urol.*, vol. 185, no. 1, pp. 148–153, Jan. 2011.
- [21] Y. Pan, G. A. Sonn, M. L. Y. Sin, K. E. Mach, M. C. Shih, V. Gau, P. K. Wong, and J. C. Liao, "Electrochemical immunosensor detection of urinary lactoferrin in clinical samples for urinary tract infection diagnosis," *Biosens. Bioelectron.*, vol. 26, no. 2, pp. 649–654, Oct. 2010.
- [22] M. L. Y. Sin, V. Gau, J. C. Liao, and P. K. Wong, "Electrothermal fluid manipulation of high-conductivity samples for laboratory automation applications," *J. Assoc. Lab. Automat.*, vol. 15, no. 6, pp. 426–432, 2010.
- [23] N. G. Green, A. Ramos, A. Gonzalez, A. Castellanos, and H. Morgan, "Electrothermally induced fluid flow on microelectrodes," *J. Electrostat.*, vol. 53, no. 2, pp. 71–87, Aug. 2001.
- [24] V. Gau, S. C. Ma, H. Wang, J. Tsukuda, J. Kibler, and D. A. Haake, "Electrochemical molecular analysis without nucleic acid amplification," *Methods*, vol. 37, no. 1, pp. 73–83, Sep. 2005.
- [25] J. C. Liao, M. Mastali, V. Gau, M. A. Suchard, A. K. Moller, D. A. Bruckner, J. T. Babbitt, Y. Li, J. Gornbein, E. M. Landaw, E. R. B. McCabe, B. M. Churchill, and D. A. Haake, "Use of electrochemical DNA biosensors for rapid molecular identification of uropathogens in clinical urine specimens," *J. Clin. Microbiol.*, vol. 44, no. 2, pp. 561–570, Feb. 2006.
- [26] M. Zuker, "Mfold web server for nucleic acid folding and hybridization prediction," *Nucleic Acids Res.*, vol. 31, no. 13, pp. 3406–3415, Jul. 2003.
- [27] C. T. Ho, R. Z. Lin, H. Y. Chang, and C. H. Liu, "Micromachined electrochemical T-switches for cell sorting applications," *Lab Chip*, vol. 5, no. 11, pp. 1248–1258, Nov. 2005.
- [28] C. M. Cheng and C. H. Liu, "An electrolysis-bubble-actuated micropump based on the roughness gradient design of hydrophobic surface," *J. Microelectromech. Syst.*, vol. 16, no. 5, pp. 1095–1105, Oct. 2007.
- [29] S. C. Chan, C. R. Chen, and C. H. Liu, "A bubble-activated micropump with high-frequency flow reversal," *Sens. Actuators A, Phys.*, vol. 163, no. 2, pp. 501–509, Oct. 2010.

**Mandy Lai Yi Sin** received the B.S. degree in physics from the University of Hong Kong, China, the M.Phil. degree in physics from the Chinese University of Hong Kong, China, and the Ph.D. degree in mechanical engineering from the University of Arizona, Tucson, AZ, USA.

She is currently a Post-Doctoral Fellow at the School of Medicine, Stanford University, Stanford, CA, USA. She is currently engaged in developing a point-of-care diagnostic device for bladder cancer. Her current research interests include electrokinetics and microfabrication for lab-on-a-chip systems.

**Vincent Gau** received the B.S. degree in electrical engineering from Tamkang University, New Taipei, Taiwan, and the M.S. and Ph.D. degrees in electrical engineering and biomedical engineering from the University of California, Los Angeles (UCLA), CA, USA.

As the first Ph.D. graduate of the Biomedical Engineering Program at UCLA, he has extensive experience and expertise in VLSI, bio-MEMS, robotic lab automation, multiplexed molecular analysis, and point of care diagnostics technologies. He is currently the President of GeneFluidics, Inc. He has been granted 23 patents in VLSI, biosensors, microfluidics technologies, and robotic systems.

**Joseph C. Liao** received the A.B. degree in biology from Harvard University, Cambridge, MA, USA, and the M.D. degree from the School of Medicine, Stanford University, Stanford, CA, USA.

He completed his post-doctoral training at the University of California, Los Angeles, CA, USA, which covered urology residency, minimally invasive surgery fellowship, and a research fellowship in BioMEMS. He is currently an Assistant Professor of urology at Stanford University, and a Board-Certified Urologic Surgeon. His current research interests include molecular diagnostics, biosensors, molecular imaging, and image-guided surgery.

**Pak Kin Wong** received the Ph.D. degree in mechanical engineering from the University of California, Los Angeles, CA, USA, in 2005.

He is currently an Associate Professor at the University of Arizona, Tucson, AZ, USA. His current research interests include mechanoregulation of collective cell behaviors and electrokinetics for clinical diagnostics.

Dr. Wong is an Editor of the *IEEE Nanotechnology Magazine*. He was a recipient of the NIH Director's New Innovator Award in 2010 and was chosen as an Arizona Engineering Faculty Fellow in 2011.